IOP Conf. Series: Materials Science and Engineering **278** (2017) 012062 doi:10.1088/1757-899X/278/1/012062

A numerical model for boiling heat transfer coefficient of zeotropic mixtures

Rodrigo Barraza Vicencio and Eduardo Caviedes Aedo

Department of Mechanical Engineering, Universidad Técnica Federico Santa María, Av. España 1680, Valparaíso, Chile

rodrigo.barraza@usm.cl

Abstract. Zeotropic mixtures never have the same liquid and vapor composition in the liquid-vapor equilibrium. Also, the bubble and the dew point are separated; this gap is called glide temperature (T_{glide}). Those characteristics have made these mixtures suitable for cryogenics Joule-Thomson (JT) refrigeration cycles. Zeotropic mixtures as working fluid in JT cycles improve their performance in an order of magnitude. Optimization of JT cycles have earned substantial importance for cryogenics applications (e.g, gas liquefaction, cryosurgery probes, cooling of infrared sensors, cryopreservation, and biomedical samples). Heat exchangers design on those cycles is a critical point; consequently, heat transfer coefficient and pressure drop of two-phase zeotropic mixtures are relevant. In this work, it will be applied a methodology in order to calculate the local convective heat transfer coefficients based on the law of the wall approach for turbulent flows. The flow and heat transfer characteristics of zeotropic mixtures in a heated horizontal tube are investigated numerically. The temperature profile and heat transfer coefficient for zeotropic mixtures of different bulk compositions are analysed. The numerical model has been developed and locally applied in a fully developed, constant temperature wall, and two-phase annular flow in a duct. Numerical results have been obtained using this model taking into account continuity, momentum, and energy equations. Local heat transfer coefficient results are compared with available experimental data published by Barraza et al. (2016), and they have shown good agreement.

1. Introduction

This research studies the thermal fluid behavior of two-phase zeotropic multi-component mixtures in small diameter horizontal tubes between cryogenic and room temperatures, with special emphasis in the evaporating process. There are few data or theories available in the open literature that can reliably predict two-phase heat transfer coefficients for the studied zeotropic mixtures operating over the wide temperature range considered here. Mixed Refrigerant Joule Thomson (MRJT) applications involve a recuperative heat exchanger with mini-channels. One side has a high-pressure boiling zeotropic mixture and the other side has the same mixture condensing with a low-pressure. The selected zeotropic mixtures for these applications experience a temperature glide around 100 K or greater.

Few studies are focused in the performance of the recuperative heat exchanger of MRJT cycles. Boiarski et al. [1], Gong et al [2], and Ardhapurkar et al. [3] have reported measurements of the overall heat transfer coefficient for a heat exchanger operating with mixtures at cryogenic temperatures. However, these data have limited utility because the overall heat transfer coefficient data cannot be extrapolated to other systems with system geometries differing from those for which the data were

Content from this work may be used under the terms of the Creative Commons Attribution 3.0 licence. Any further distribution of this work must maintain attribution to the author(s) and the title of the work, journal citation and DOI.
Published under licence by IOP Publishing Ltd

obtained. Ardhapurkar et al. [4] have measured the overall heat transfer coefficient in a helical coiled heat exchanger of a MRJT system. A multi-component mixture of nitrogen–hydrocarbons undergo evaporation in one side and condensation in the other side. The measured overall heat transfer coefficient is compared with a calculated overall heat transfer coefficient that utilizes condensation correlations for pure fluids and small glide zeotropic mixtures because of the unavailability of data. Alexeev et al. [5] numerically studied multi tubes-in-tube heat exchanger for different mixture compositions. Chen correlation is used to calculate the heat transfer coefficients for forced convection, as well as for condensation of mixtures; however, the calculated results were not compared with experimental data. Nellis et al. [6] and Barraza [7] have provided some experimental data for local heat transfer coefficients of boiling zeotropic mixtures used in MRJT applications. These are probably the only two experimental studies on the flow boiling of zeotropic mixtures at cryogenic temperatures.

Nellis provides six sets of data for the local heat transfer coefficient during boiling of nitrogen-hydrocarbon gas zeotropic mixtures evaporating in a horizontal test section with an inner diameter of 0.835 mm over a range of composition, temperatures, mass fluxes, and pressures. The zeotropic mixtures are formed by different compositions of nitrogen, methane, ethane, propane and isobutane. The test conditions include variation of mass flux between 200 and 900 kg/m2-s, evaporating pressures between 400 and 1400 kPa. A constant heat flux of 80 kW/m2 is used for all test conditions. Barraza shows 36 set of zeotropic mixtures formed by two (binary), three (ternary), four (quaternary) and five (quinary) component mixtures. These zeotropic mixtures include hydrocarbons (methane, ethane, and propane) and synthetic mixtures (R-14, R-23, R-32, and R-134a). The sensitivity of the measured heat transfer coefficient to parameters such as heat flux (18 - 87 kW/m^2), mass flux (144 - 240 kg/s-m^2), pressure (270 and 790 kPa), tube diameter (0.5, 1.5, and 3.0 mm), and mixture composition (diluting with nitrogen and argon) is also presented. The boiling heat transfer coefficients results suggest that the heat transfer process is driven, principally, by convective boiling; however, composition, diameter, and surface roughness affect the measured heat transfer coefficients. Evaporating pressure has less relevance compared to the other parameters.

Although Nellis et al. [6] and Barraza et al [8] have provided some data for the boiling process, the heat transfer process experienced by boiling multi-component mixtures at cryogenic temperatures in microchannel heat exchangers is not fully understood. In this work, the flow and heat transfer characteristics of zeotropic mixtures in a heated horizontal tube are investigated numerically. A methodology based on the law of the wall approach for turbulent flows is applied in order to calculate the local convective heat transfer coefficients.

2. Numerical model

This study proposes to analyze zeotropic mixtures during boiling as they flow through horizontal minitubes. It is suggested that zeotropic mixtures under the analyzed conditions show annular flow condition in most of the two-phase region as they evaporate [8]. The liquid and vapor phases are modeled using the velocity profile suggested by Van Driest [9] that assume that both phases are hydrodynamically fully developed. It is assumed no slip condition in both interfaces: between the liquid film and ($u_{l,y=o} = 0$) the wall and between the vapor core and the liquid film ($u_{l,y=\delta} = u_{v,y=\delta}$). An uniform initial temperature is given to the inlet flow. The flow is exposed to a hotter uniform wall temperature; consequently, the two-phase flow begins to be warmer as it flows axially through the pipe. It is expected to study the heat transfer process when a thermally fully developed condition is achieved. The fully developed condition is obtained when the Nusselt number does not change anymore. The local thermodynamic and transport properties for the gas mixtures are calculated using REFPROP by Lemmon et al. [10].

2.1. Shear stress

The liquid film flows through the pipe surrounding the vapor core and wetting the inlet wall pipe. The void fraction correlation proposed by Rouhanni and Axelsson [11] is used to determine the section areas occupied by the liquid and the vapor. The force balances experienced by both phases are shown in Figure 1. The force balances allow to determine the shear stress in both interfaces: liquid-wall and vapor-liquid. The shear stress at the vapor-liquid interface is calculated by means of the force balance in the vapor. Subsequently, the shear stress at the wall is determined by a force balance in the liquid.

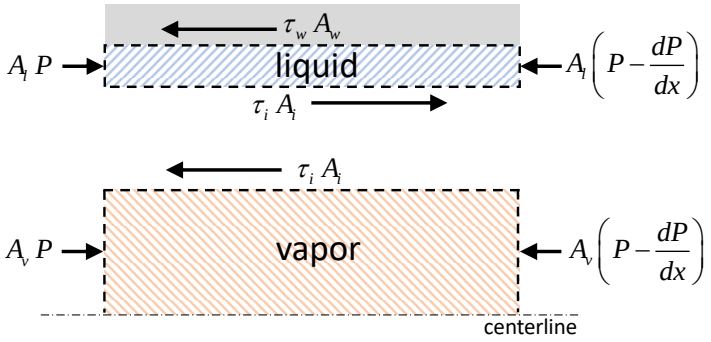

Figure 1. Force balance

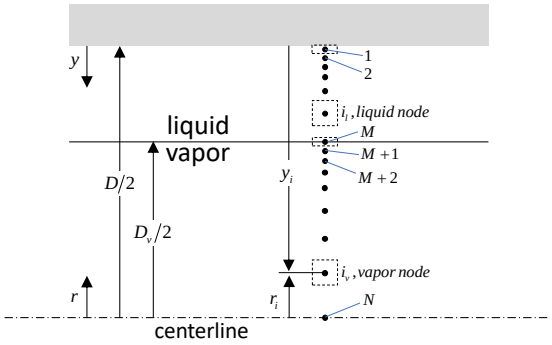

Figure 2. Discretization in liquid and vapor phases.

2.2. Velocity profile and discretization

The liquid film flowing between the tube wall and the vapor is modeled using the universal velocity distribution (u^+) proposed by Van Driest [9] for turbulent flow. Also, the same velocity distribution is used to represent the vapor core. Equations 1 and 2 show the velocity gradient (du^+/dy^+) and the associated eddy diffusivity (ε_M/υ) model proposed by Van Driest.

$$\frac{du^+}{dy^+}=\frac{2}{1+\sqrt{1+4\left(0.41y^+\right)^2\left[1-\exp\left(-y^+/26\right)\right]^2}} \tag{1}$$

$$\frac{\varepsilon_M}{\upsilon}=\left\{0.41y^+\left[1-\exp\left(-y^+/24.7\right)\right]\right\}^2\left|\frac{du^+}{dy^+}\right| \tag{2}$$

The velocity profiles for both phases show an important variation near the interfaces. The shear stress is transmitted according to the friction velocity ($u*$) and is a function of the shear stress (τ) and the fluid density (ρ). Equation 3 shows the friction velocity ($u*$).

$$u^* = \sqrt{\frac{\tau}{\rho}} \tag{3}$$

The viscous sublayer is represented by the characteristic length (L_{char}) presented in equation 4. Where ν is the kinematic viscosity.

$$L_{char} = \frac{\nu}{u^*} \tag{4}$$

Both quantities (u^* and L_{char}) are calculated for both phases. The discretization representation for both phases is shown in Figure 2. The liquid and vapor phases are indicated using the subscripts *l* and *v*, respectively. More nodes are located near the interfaces to consider shear stress effects on these regions. Equation 5 shows the multiplicative factor (*MF*) used to define the node distribution for both phases. The proposed MF allows setting up the nodal network in a logarithmic-spacing fashion.

$$MF = \begin{cases} \left(\frac{\delta}{L_{char,l}}\right)^{\frac{1}{M-1}}, \ for\ liquid \\ \left(\frac{D_i}{2L_{char,v}}\right)^{\frac{1}{N-M-1}}, \ for\ vapor \end{cases} \tag{5}$$

M is the numbers of nodes in the liquid region, N is the total number of node, and δ is the liquid film thickness ($(D - D_i)/2$). The dimensionless position (y_i^+) is defines as shown in equation 6.

$$y_i^+ = \begin{cases} MF_i^{i-1}, \ if\ i < M \\ MF_v^{i-(M+1)}, \ if\ M+1 < i < N \end{cases} \tag{6}$$

Finally, the position (y_i) inside of the pipe is obtained combining the dimensionless position (y_i^+) and the characteristic length (L_{char}) of the viscous sublayer (equation 7). $y = 0$ is defines on the wall pipe and $y = D/2$ at the center of the pipe.

$$y_i = \begin{cases} y_i^+ L_{char,l}, \ if\ i < M \\ y_i^+ L_{char,v} + \delta, \ if\ M+1 < i < N \end{cases} \tag{7}$$

The axial discretization to take into account the development of the thermal boundary layer is defined by equation 8.

$$\Delta x = L/n_{axial} \tag{8}$$

Where Δx is the length of the axial discretization, L is the length where the thermally fully development condition is achieved, and n_{axial} is the number of axial discretizations. In this case, it is defined $L = 10D$ and $n_{axial} = 2500$.

2.3. Energy balances in nodes

An effective thermal conductivity is calculated for each node that considers the molecular diffusivity and the eddy diffusivity due to turbulence. Equation 9 shows the effective thermal conductivity ($k_{eff,i}$) for each node.

$$k_{eff,i} = k + \frac{\nu \rho c}{\mathrm{Pr}_{turb}} \left(\frac{\varepsilon_M}{\upsilon}\right)_i \tag{9}$$

where k is the thermal conductivity, ν is the kinematic viscosity, ρ is the density, *c* is the specific heat, and Pr_{turb} is the turbulent Prandtl number. In this case, the turbulent Prandtl number is selected to be $\mathrm{Pr}_{turb} = 0.9$.

On each node an energy balance is performed. The most important nodes and their energy balances are shown in Figure 3. Figure 3a shows the node that is next to the wall pipe. The energy balance for this first node is shown in equation 10.

$$\rho_l\, c_l\, u_1\, A_{c,1}\, T_1 + \dot{q}_{in} + \dot{q}_{wall} = \rho_l\, c_l\, u_1\, A_{c,1}\, T_1 + \rho_l\, c_l\, u_1\, A_{c,1}\, \frac{dT_1}{dx}\Delta x \tag{10}$$

The first node experiences energy transfer from four directions. In the radial direction, the first node receives heat from the wall ($\dot{q}_{wall}$) as shown in equation 11.

$$\dot{q}_{wall} = k_{eff,1}\, \pi D \Delta x \frac{\left(T_{wall} - T_1\right)}{\left(D/2 - r_1\right)} \tag{11}$$

Also, the first node receives energy from the node 2 ($\dot{q}_{in}$) in the radial direction, equation 12.

$$\dot{q}_{in} = \frac{\left(k_{eff,1} + k_{eff,2}\right)}{2} 2\pi \frac{\left(r_1 + r_2\right)}{2} \Delta x \frac{\left(T_2 - T_1\right)}{\left(r_1 - r_2\right)} \tag{12}$$

The radial energy addition ($\dot{q}_{wall}$ and $\dot{q}_{in}$) increases the temperature of the axial flow. The increment of temperature on the axial direction is determined combining equations 10-12 and is shown in equation 13.

$$\frac{dT_1}{dx} = \frac{1}{\rho_l\, c_l\, u_1\, A_{c,1}} \left[\frac{\left(k_{eff,1} + k_{eff,2}\right)}{2} 2\pi \frac{\left(r_1 + r_2\right)}{2} \frac{\left(T_2 - T_1\right)}{\left(r_1 - r_2\right)} + k_{eff,1}\, \pi D \frac{\left(T_{wall} - T_1\right)}{\left(D/2 - r_1\right)} \right] \tag{13}$$

The interface nodes are shown in Figures 3c and 3d. An energy balance on the liquid interface node (Figures 3c) is used to determine the increment of temperature of the axial flow leaving the interfacial liquid node. The heat addition is produce by the influence of the radial energy addition from the liquid node *M-1* ($\dot{q}_{out}$) and from the vapor node *M+1* ($\dot{q}_{in}$). Also, the evaporation is accounted as a heat dissipation on the liquid-vapor interface ($\dot{q}_{evap}$). Similar procedure is used for the other nodes.

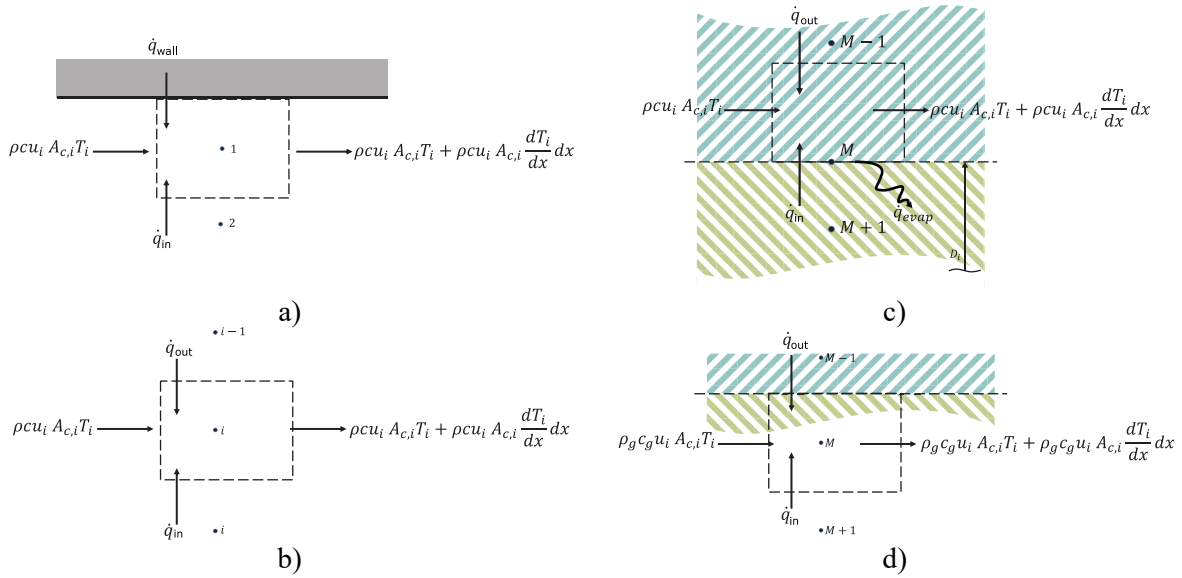

Figure 3. Nodal energy balances. a) First node next to the wall, b) general node "i", c) interfacial node for the liquid, and d) interfacial node for the vapor.

3. Heat transfer model

The numerical model provides enough information to estimate the heat transfer coefficient for the two-phase flow mixture. This approach just assumes that the heat transfer of the two-phase mixture occurs across the conductive viscous sublayer of the turbulent liquid film as suggested by Hurlburt and Newell [12]. Consequently, the heat transfer coefficient may be obtained knowing the bulk temperature of the liquid (equation 14).

$$htc = \frac{\dot{q}''}{T_{wall} - T_l} \tag{14}$$

The bulk temperature of the liquid may be obtained averaging the sum over the bulk flow as indicated in equation 15.

$$T_l = \frac{\dot{1}}{u_l A_l} \sum_{i=1}^{M} \left(u_i A_i T_i \right) \tag{15}$$

4. Model validation

The numerical model is validated using some of the data provided by Barraza [7]. Table 1 shows the experimental data selected for hydrocarbon mixtures. Binary (methane and ethane), ternary (methane, ethane, and propane), and quaternary mixtures (methane, ethane, propane, and nitrogen) are selected. The tested pipe diameter is 2.87 mm and the tested pressure is around 788 kPa. Heat flux, mass flux, and composition are changed. The experimental heat transfer coefficient shows two-phase behavior between a thermodynamic quality of 10 and 90%.

Table 1. Experimental data from Barraza et al. [7].

Run	Mixture	D *m*	P *kPa*	G *kg/m²-s*	q" *kW/m²*
12	45%CH_4\35%C_2H_6\20%C_3H_6	2.871	791	147	40
13	45%CH_4\35%C_2H_6\20%C_3H_6	2.871	790	146	56
14	36%CH_4\28%C_2H_6\16%C_3H_6\20%N_2	2.871	791	147	58
15	27%CH_4\21%C_2H_6\12%C_3H_6\40%N_2	2.871	790	147	58
36	40%CH_4\60%C_2H_6	2.871	785	147	40
37	40%CH_4\60%C_2H_6	2.871	788	147	57

5. Results

The velocity and temperature profile are shown in Figure 4 for a ternary hydrocarbon mixture (Run 12) as a function of the radius. It is clear the liquid profile closer to the wall and the vapor profile in the center. Both profiles are shown for a thermodynamic quality of 25, 50, and 75%.

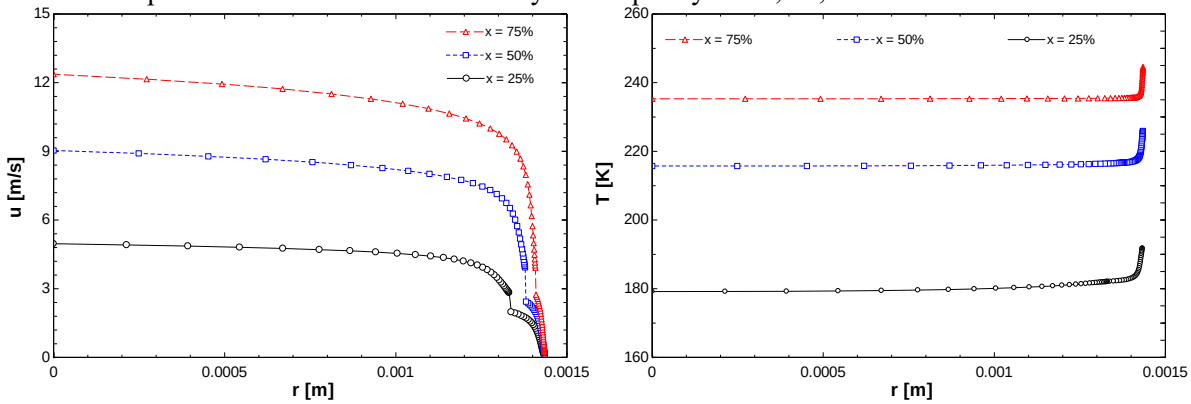

Figure 4. Velocity and temperature profiles (Run 12), x = 25, 50, and 75%.

The numerical model is used to predict heat transfer coefficient for zeotropic mixtures (hydrocarbons) experiencing boiling at the range of thermodynamic quality between 10 and 90%. Figure 5 shows a comparison between the experimental data (Run 37) and the predicted data. The model is in good agreement for thermodynamic qualities above ~20%.

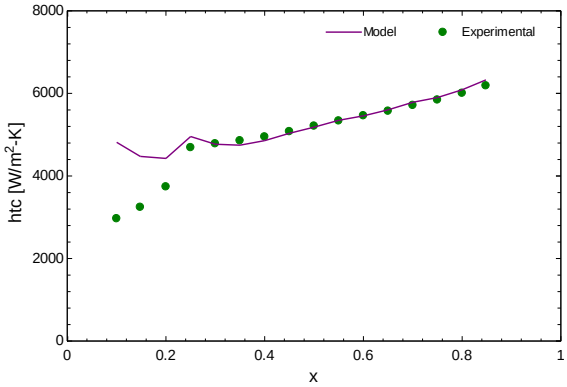

Figure 5. Experimental and predicted heat transfer coefficient for a binary hydrocarbon mixture (Run 37).

The numerical model is tested against the experimental data indicated in Table 1. Figure 6 (left) presents the experimental data versus the predicted heat transfer coefficients. Most of the predicted values are in +/-20% of the experimental data. The average absolute deviation is lower than 16% for the tested data. Most of the point out of the +/-20% correspond to the Run 15, which contains 40% of Nitrogen. On Run 15, the model shows important difference in comparison with experimental data for qualities below 35%. Figure 6 (right) shows the relative error as a function of thermodynamic quality. Clearly the model fails to accurately predict the heat transfer coefficients below thermodynamic qualities ~20%. The model still does a great job of predicting the heat transfer coefficients for a wide range of values of qualities above 20%.

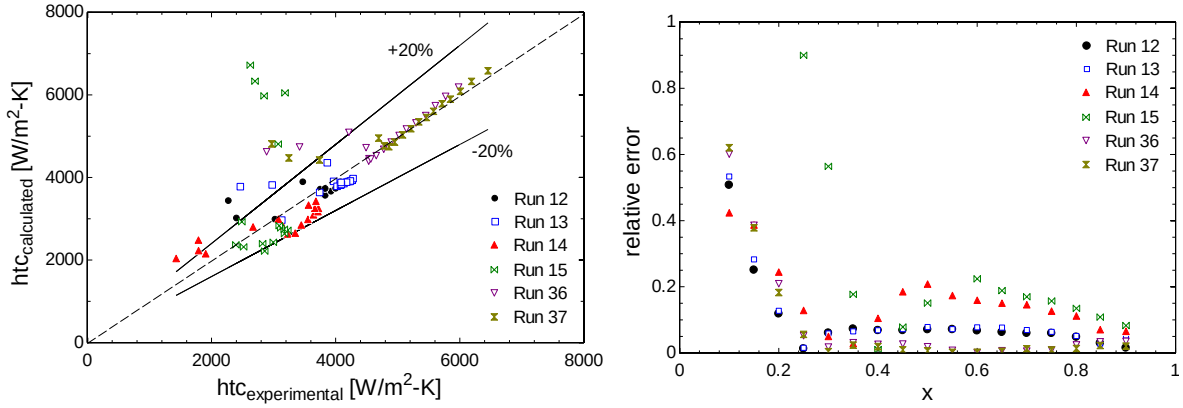

Figure 6. Experimental and predicted heat transfer coefficient for a binary hydrocarbon mixture (Run 37).

6. Conclusions

A numerical model that allows to determine the local convective heat transfer coefficients of boiling zeotropic mixtures have been developed. The model is based on the law of the wall approach for hydrodinamically developed turbulent flows. The velocity profile suggested by Van Driest has been used. The model considers continuity, momentum, and energy equations. The heat transfer process for the analyzed hydrocarbon mixtures seems to occur across the conductive viscous sublayer of the

turbulent liquid film. The numerical model has been compared against the local heat transfer coefficient data published by Barraza [7]. The model shows good agreement with the experimental data with an average absolute deviation below 16%.

7. References

[1] Boiarski M, Khatri A and Kovalenko V 2002 Design Optimization of the Throttle-Cycle Cooler with Mixed Refrigerant *Cryocoolers 10* ed R G R Jr (Springer US) pp 457–65
[2] Gong M Q, Wu J F, Luo E C, Qi Y F, Hu Q G and Zhou Y 2002 Study on the overall heat transfer coefficient for the tube-in-tube heat exchanger used in mixed-gases coolers *AIP Conference Proceedings* ADVANCES IN CRYOGENIC ENGINEERING: Proceedings of the Cryogenic Engineering Conference - CEC vol 613 (AIP Publishing) pp 1483–90
[3] Ardhapurkar P M, Sridharan A and Atrey M D 2014 Experimental investigation on temperature profile and pressure drop in two-phase heat exchanger for mixed refrigerant Joule–Thomson cryocooler *Appl. Therm. Eng.* **66** 94–103
[4] Ardhapurkar P M, Sridharan A and Atrey M D 2014 Performance evaluation of heat exchanger for mixed refrigerant J–T cryocooler *Cryogenics* **63** 49–56
[5] Alexeev A, Thiel A, Haberstroh C and Quack H 2000 Study of behavior in the heat exchanger of a mixed gas Joule-Thomson cooler *Adv. Cryog. Eng.* **45** 307–314
[6] Nellis G, Hughes C and Pfotenhauer J 2005 Heat transfer coefficient measurements for mixed gas working fluids at cryogenic temperatures *Cryogenics* **45** 546–56
[7] Barraza R S 2015 *Thermal-Fluid Behavior of Mixed Refrigerants for Cryogenic Applications* Dissertation (University of Wisconsin-Madison)
[8] Barraza R, Nellis G, Klein S and Reindl D 2016 Measured and predicted heat transfer coefficients for boiling zeotropic mixed refrigerants in horizontal tubes *Int. J. Heat Mass Transf.* **97** 683–95
[9] Nellis G and Klein S 2008 *Heat Transfer* (New York: Cambridge University Press)
[10] Lemmon E W, Huber, Marcia L. and McLiden, Mark O. 2014 *REFPROP* (NIST Standard Reference Database 23)
[11] Rouhani S Z and Axelsson E 1970 Calculation of void volume fraction in the subcooled and quality boiling regions *Int. J. Heat Mass Transf.* **13** 383–93
[12] Hurlburt E T and Newell T A 1999 Characteristics of Refrigerant Film Thickness, Pressure Drop, and Condensation Heat Transfer in Annular Flow *HVACR Res.* **5** 229–48